



Photocatalytic degradation of Acridine orange dye and real textile wastewater via ZnO nanoparticle supported natural Tunisian clay

M. Ibn Mahrsi^a, S. Khelifi^a, R. Alcharary^b, A. Berez^b, L. Mansour^c, F. Ayari^{a,*}

^aFaculty of Sciences of Bizerte, LR 05/ES09 Laboratory of Applications of Chemistry to Resources and Natural Substances and to the Environment (LACReSNE), Carthage University, Zarzouna 7021, Tunisia, emails: fadhilaayari@yahoo.fr (F. Ayari), selma.khelifi@gmail.com (S. Khelifi)

^bLaboratoire d'Hydrologie et de Géo chimie de Strasbourg (LHyGeS) - UMR 7517 Centre National de Recherche Scientifique, Université de Strasbourg, 1 rue Blessig, 67084 Strasbourg Cedex, France, emails: reemalsharary@yahoo.fr (R. Alcharari), berz.amor@yahoo.fr (A. Berez)

^cZoology Department, College of Science, King Saud University, Riyadh, Saudi Arabia, email: lmansour@ksu.edu.sa (L. Mansour)

Received 25 October 2021; Accepted 18 April 2022

ABSTRACT

Decontamination of dye molecules from polluted water through photocatalyse process is reported to be a performing technology. In this study, sol gel synthesis route was used to prepare ZnO nanoparticles and ZnO modified natural and abundant bentonitic clay. ZnO and ZnO-clay nanocomposites were characterized by X-ray diffraction, Fourier-transform infrared spectroscopy, N₂ adsorption–desorption, transmission electron microscopy techniques and tested for Acridine orange dye photodegradation using artificial UV irradiation. Experimental data indicates that ZnO-clay was an efficient photocatalyst under UV irradiation and in the presence of H₂O₂ oxidant (around 97.8% of Acridine orange removal and 82.7% mineralization were achieved after 90 min). Adsorption experiments were studied and both pseudo-second-order and pseudo-first-order for kinetics models fitted the Acridine orange adsorption data except with pure ZnO catalyst adsorption process is described only by pseudo-second-order model. Photocatalytic degradation data of Acridine orange followed the first-order removal rate with three materials: pure clay, ZnO and ZnO-clay and the apparent rate constant increased with photocatalyst performance. The mechanistic detail of the dye photodegradation was studied via the separation and identification of the products intermediates by liquid chromatography–mass spectrometry method. Obtained results suggested that the N-de-methylation mechanism of Acridine orange (AO) dye took place leading to the generation of mono-, di-, tri-, and tetra-N-de-methylated AO products during the reaction. Synthetic photocatalyst ZnO-clay was reused three times without an apparent decrease in its degradation efficiency even after 3 runs (94.7% of AO removal), proving the high stability and reutilisability. As well, ZnO-clay was tested in the treatment of a real textile effluent and obtained results (80.6% of effluent mineralization) confirm its great performance in the environmental decontamination.

Keywords: Photocatalyse; ZnO-clay; Acridine orange; Mineralization; Liquid chromatography–mass spectrometry; separation; UV irradiation

1. Introduction

Industries such as petrochemical, food, and textile produce huge quantities of highly charged effluents, hardly

biodegradable and generally bio-recalcitrant [1]. Textile industry is one of the most water-consuming industries [2,3]. Also, it generates recalcitrant and toxic organic molecules which are responsible of organoleptic and aesthetic

* Corresponding author.

pollution, causes health problems and contaminates ground-water, soil and vegetation [4,5].

Acridine orange dye (3,6-bis(dimethylamino)acridine), is a cationic dye, used as fluorescence dye in molecular biology, toxicology, and supramolecular chemistry [6]. It is often used to probe DNA structure in drug-DNA and protein-DNA interactions [7]. It is difficult to biodegrade this dye due to its complex aromatic structure and also, it was considered as toxic and carcinogenic compound [8,9]. For this reason, some researchers were reported in the literature for Acridine orange dye removal: Jauris et al. [10] were studied the efficiency of carbon nanotubes for the adsorptive removal of Acridine orange dye. Nejad-Darzi et al. [11] were interested in the adsorption of Acridine orange using ZSM-5 nanozeolithe as adsorbent. Also, several physical processes have been envisaged for industrial wastewater treatment before discharge, in particular membrane filtration [12], precipitation/coagulation of dyestuffs [13] and adsorption on activated carbon [14]. But, these methods have the disadvantage of moving simply pollution in large amounts of sludge [15]. It is therefore necessary to create and implement simple and inexpensive solutions in order to treat industrial effluents.

The researchers concentrated their efforts on more powerful oxidation processes: the advanced oxidation processes (AOPs). These technologies have already shown their potential in the treatment of bio-recalcitrant organic pollutants [16,17]. Many authors use these technologies in the treatment of textile effluent: H_2O_2/UV [18]; TiO_2/UV [19,20]; $TiO_2/H_2O_2/UV$ [21]; homogeneous Fenton reaction [22] and homogeneous photo-Fenton reaction [23]. However, the costs involved with the energy requirements and chemicals, especially when complete mineralization is the main objective, are expensive and eventually make these processes inapplicable at the industry scale [24]. Photocatalysis is among the powerful Acridine orange (AO) techniques and it was the subject of many studies; it remains very promising by its ability to destroy organic compounds into simple molecules like CO_2 , H_2O , and mineral acids [25]. Also, it is based on the high photocatalytic activity of the used catalyst. Then, many authors have been attempted the photodegradation of dye molecules by means of different photocatalysts such as TiO_2 [26], ZnO [6], pillared clay [27], and iron oxide [28].

The development of newer eco-friendly methods able to destroy these pollutants has become an imperative task such as photocatalyse process using ZnO modified clay as

heterogeneous photocatalyst and UV irradiation as light source. In this sense, the main objective of the present work is to study the activity of raw Tunisian clay (bentonite) before and after modification with ZnO, using sol-gel route, in the photodegradation and mineralization of Acridine orange cationic dye in aqueous solution followed by phototreatment of real textile effluent collected from Tunisian Textile Company.

2. Materials and methods

2.1. Chemicals and products

Pollutant used in this study is a cationic dye: Acridine orange (AO) (Table 1), a dark orange powder belongs to acridine dye family [6].

Clay used in this study is natural sodic smectite collected from the soil of "Gafsa" situated in the south of Tunisia.

All other chemicals used in this work were of analytical grade and were used without any further purification: zinc acetate dihydrate ($Zn(C_2COO)_2 \cdot 2H_2O$), ethanol, triethanolamine, and H_2O_2 (35%).

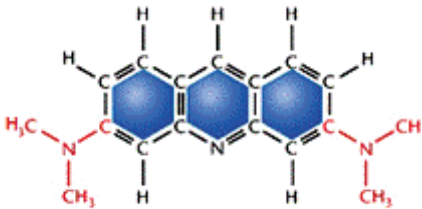
2.2. Photocatalysts preparation

ZnO nanoparticles and ZnO-clay nanocomposites were synthesized by sol-gel route as described in previous work by Hadjltaief et al. [29]: 4.38 g of dehydrated zinc acetate were dissolved in 100 mL of ethanol and stirred in a water bath at 50°C. Then, 2.98 g of tri-ethanolamine were subsequently added to the solution while stirring was continued for 1 h. The mixture was placed under vibration and heated for 30 min at 40°C, conducting to a colorless and transparent sol. After that, 3 g of clay were added to this sol. The resulted suspension was agitated under vibration for 30 min, filtered, dried for 12 h, and calcined at 300°C for 4 h.

2.3. Characterization of the investigated materials

Mineralogical analysis was conducted by X-ray diffraction (XRD) using PANalytical X'Pert HighScorePlus diffractometer, CuK_α radiation ($\alpha = 1.5406 \text{ \AA}$) source. Isotherm of nitrogen adsorption-desorption of the material was measured using Quantachrome model Nova 1000^e surface and porosity analyzer. The specific surface area (S_{BET}) was obtained by the Brunauer-Emmett-Teller (BET) method and the total pore volume (V_p) was calculated at a relative N_2 pressure of $P/P_0 = 0.99$ at liquid nitrogen temperature of

Table 1
Chemical structure and properties of Acridine orange dye (AO)

Molecular structure	Empirical formula	Molecular weight (g mol ⁻¹)	λ_{max} (nm)	Solubility in water
	$C_{17}H_{19}N_3$	369.94	490	1 mg mL ⁻¹

196°C. Fourier-transform infrared spectroscopic data was determined using Perkin Elmer 783 dispersive spectrometer in the range of 4,000–400 cm⁻¹. Transmission electron microscopy (TEM) was analyzed to define the morphology of pure clay before and after modification with ZnO nanoparticles.

2.4. Adsorption tests

Batch experiments with the studied pollutant were carried out to investigate the adsorption efficiency of the selected photocatalysts and to define the kinetic model and adsorption process.

Adsorption measurements were performed in 250 mL glass vessels containing 100 mg of adsorbent and 100 mL of adsorbate without pH solution adjustment and at room temperature (25°C). Effect of contact time was studied varying it from 10 to 120 min. Suspension from each sample was immediately centrifuged and filtered using a 0.45 mm syringe filter.

The amount of remaining AO dye in the solution was determined by UV-Visible spectrometer (Shimadzu Model Perkin Elmer) at maximum absorbance 490 nm.

Adsorption percent (% adsorption) was calculated as follows:

$$\% \text{ Adsorption} = \frac{C_0 - C_t}{C_0} \times 100 \quad (1)$$

The adsorption capacity (Q_{ads}) was calculated using Eq. (2):

$$Q_{\text{ads}} = \frac{(C_0 - C_t)V}{m} \quad (2)$$

where C_0 : initial dye concentration, C_t : dye concentration at time t , m : mass of the adsorbent used (g) and V : volume of dye solution (L).

Kinetic modeling was assumed to the pseudo-first-order and the pseudo-second-order given as follow:

The pseudo-first-order equation [30]:

$$\ln(q_e - q_t) = \ln q_e - K_1 t \quad (3)$$

where q_e is the amount of adsorbate adsorbed (mg g⁻¹) at equilibrium, q_t is the amount of adsorbate adsorbed (mg g⁻¹) at time t (min) and K_1 (min⁻¹) is the pseudo-first-order rate constant. These kinetic parameters were determined from the slope and intercept of the linear presentation of $\ln(q_e - q_t)$ vs. t .

The pseudo-second-order equation [31]:

$$\frac{t}{q_t} = \frac{1}{K_2 q_e^2} + \frac{1}{q_e} t \quad (4)$$

where K_2 (min⁻¹) is the pseudo-second-order rate constant. Kinetic parameters were determined from the slope and intercept of the linear presentation of t/q_t vs. t .

2.5. Photocatalytic tests

2.5.1. Photo-reactor presentation

The photocatalytic reaction was carried out in a lab-scale photoreactor illuminated with UV lamp. The photo-reactor used is a Pyrex cylinder with 150 mL of volume. A magnetic stirrer was provided to ensure complete homogenization of the solution inside the glass vessel. Irradiation was provided by a 125 W Philips HPK UV-lamp (UV-A) placed in a plugging tube. A Pyrex cylindrical jacket located around the plugging tube allows an irradiation with wavelength $\lambda = 350$ nm.

2.5.2. Experimental run

All experiments were done at room temperature ($T = 25^\circ\text{C}$) and without pH regulation (natural pH of Acridine orange dye solution). The photo-reactor was filled with 150 mL of AO dye (10^{-4} M), the desired amount of photocatalyst (0.2 g) was added and then, the suspension was homogenized during 1 h in the darkness to ensure adsorption-desorption equilibrium. The lamp was turned ON and the solution was completely exposed to the UV light irradiations. Finally, 1 mL of hydrogen peroxide (30%) was added in the case of photocatalyst/UV/H₂O₂ system. Samples were taken at pre-defined times to evaluate degradation process, centrifuged and filtered.

The photodegradation rate (%) in each solution was determined by UV-Vis spectrophotometer (Shimadzu Model Perkin-Elmer), absorbance measurements were performed at the maximum wavelength of AO dye ($\lambda_{\text{max}} = 490$ nm). Dye mineralization efficiency was estimated by chemical oxygen demand (COD) concentration measurement using HACH LANGE DR3900.

The separation and the identification of the product intermediates were investigated by liquid chromatography-mass spectrometry (LC-MS) technique. LC was carried out on an AtlantisTM dC₁₈ column. The flow rate of the mobile phase was set at 1×10^{-3} L min⁻¹. Two solvents were used: solvent A was 25 mM of aqueous ammonium acetate buffer (pH = 6.9), solvent B was methanol. The column effluent was introduced into the ESI source of the mass spectrometer.

3. Results and discussion

3.1. Clay description

Starting clay used for ZnO-clay synthesis underwent a purification stage before the nanocomposite synthesis for solid impurities removal. Sedimentation was used for quartz elimination and several drops of HCl were added into the clay suspension to dissolve the CO₃²⁻. Pure clay was collected by centrifugation and washed with deionised water. And finally sample was ground and sieved at 63 µm.

Physicochemical properties of starting clay was determined as described in our previous work [27], it is a natural sodic smectite with BET surface area (S_{BET}) of 68 m² g⁻¹ and cation exchange capacity (CEC) of 72.7 meq/100 g. Chemical composition of this sample is: 17.1% Al₂O₃, 43.4% SiO₂, 5.82% Fe₂O₃, 2.04% MgO, 12.67% CaO, 1.13% Na₂O, 1.08% K₂O.

3.2. Photocatalysts characterization

3.2.1. XRD analysis

X-ray diffraction patterns for pure clay, ZnO and ZnO-clay are presented in Fig. 1. Results show peak at 12.6 Å proving that the studied sample is a smectite naturally sodic [32]. Peaks at 7.11 and 3.57 Å suggested the presence of kaolinite phase [32].

XRD patterns of ZnO nanoparticles shows strong diffraction peaks at 32°, 34°, 37°, 47°, 56°, 58°, 63°, 68°, 96°, 72°, and 78° corresponding respectively to (100), (002), (101), (102), (110), (103), (200), (112), (201), (004), and (202) reflections of zincite according to the standardized JCPDS file number 750526 [33]. The ZnO-clay diffractogram, beside to clay diffraction peaks, presents news peaks observed at 2θ equal to 32°, 34°, 36°, 47°, 55°, and 63° pointing the presence of hexagonal zincite phase of ZnO in this nanocomposite [34]. Furthermore, we noted that d_{001} reflection moves from 12.6 to 13.6 Å after ZnO modification recommended the success of ZnO intercalation into the interlayer smectite space.

3.2.2. Surface analysis and porosity

Textural property of photocatalyst is an important parameter to characterize the material. Table 2 presents the specific surface area (S_{BET}) and total pore volume (V_p) of studied materials.

After ZnO intercalation specific surface area of pure clay increases from 72 to 120 $\text{m}^2 \text{g}^{-1}$ and the total pore volume increases considerably from 0.07 to 0.14 $\text{cm}^3 \text{g}^{-1}$. These results reveal amelioration of textural property of this nanocomposite and suggest the existence of porous ZnO phase on the clay surface which enhances the adsorptive and the photocatalytic activities of ZnO-clay. Similar results were obtained by Hadjitaief et al. [35].

3.2.3. Transmission electron microscopy

TEM micrographs show the internal structure and give an accurate detection of particle sizes. As can be seen in Fig. 2b, ZnO nanoparticles were almost spherical in shapes with a particle size range from 31 to 210 nm. Also, after ZnO modification, pure clay (Fig. 2a) shows an important change in morphology (Fig. 2c). The TEM outcome was consistent with the XRD results, confirming the dispersion of ZnO particles in the clay surface.

3.2.4. Fourier-transform infrared spectroscopy analysis

IR spectra of synthesized ZnO nanoparticles, ZnO-clay, and pure clay (Fig. 3) showed a characteristic peak of Zn–O binding at 430 cm^{-1} in ZnO spectrum [35]. In the pure clay spectrum, the broad band's at around 3,419 cm^{-1} (H–O–H stretching) and 1,646 cm^{-1} (H–O–H bending) indicate the presence of adsorbed water. The presence asymmetric stretching mode of Si–O–Si was suggested by the absorption bands at the range of 1,035–1,123 cm^{-1} [36]. Asymmetric and symmetric bending modes of O–Si–O were observed at 536 and 469 cm^{-1} [36], these bands appears also in ZnO-clay spectrum yet we noted that bands at 3,630 and 3,440 cm^{-1} was broaden, in comparison with those in pure clay, due to a single bond of OH groups with the ZnO inserted in the clay mineral [37].

Table 2
Textural properties of pure clay, ZnO and ZnO-clay

	Pure clay	ZnO	ZnO-clay
S_{BET} ($\text{m}^2 \text{g}^{-1}$)	68	9.2	120
V_p ($\text{cm}^3 \text{g}^{-1}$)	0.07	0.06	0.14

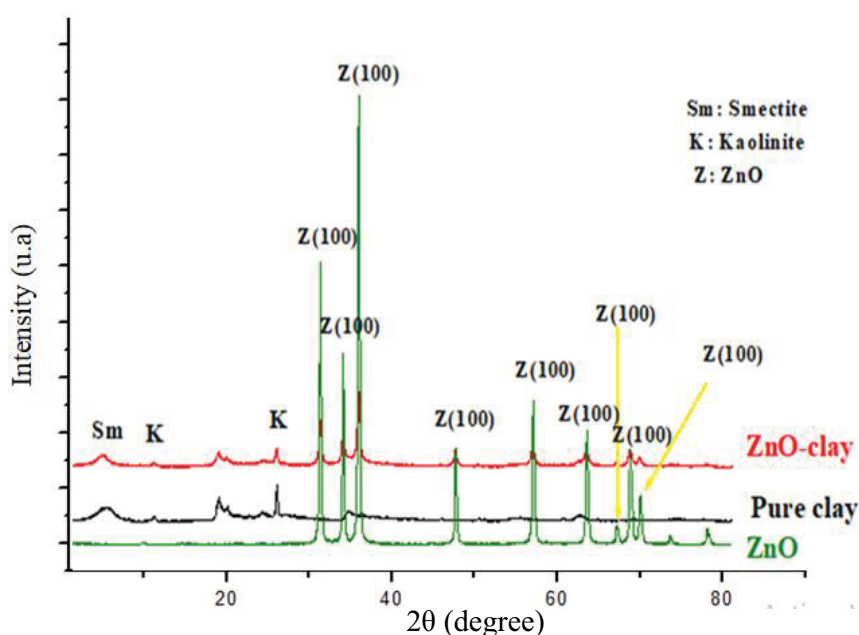


Fig. 1. XRD patterns of pure clay, ZnO and ZnO-clay photocatalysts.

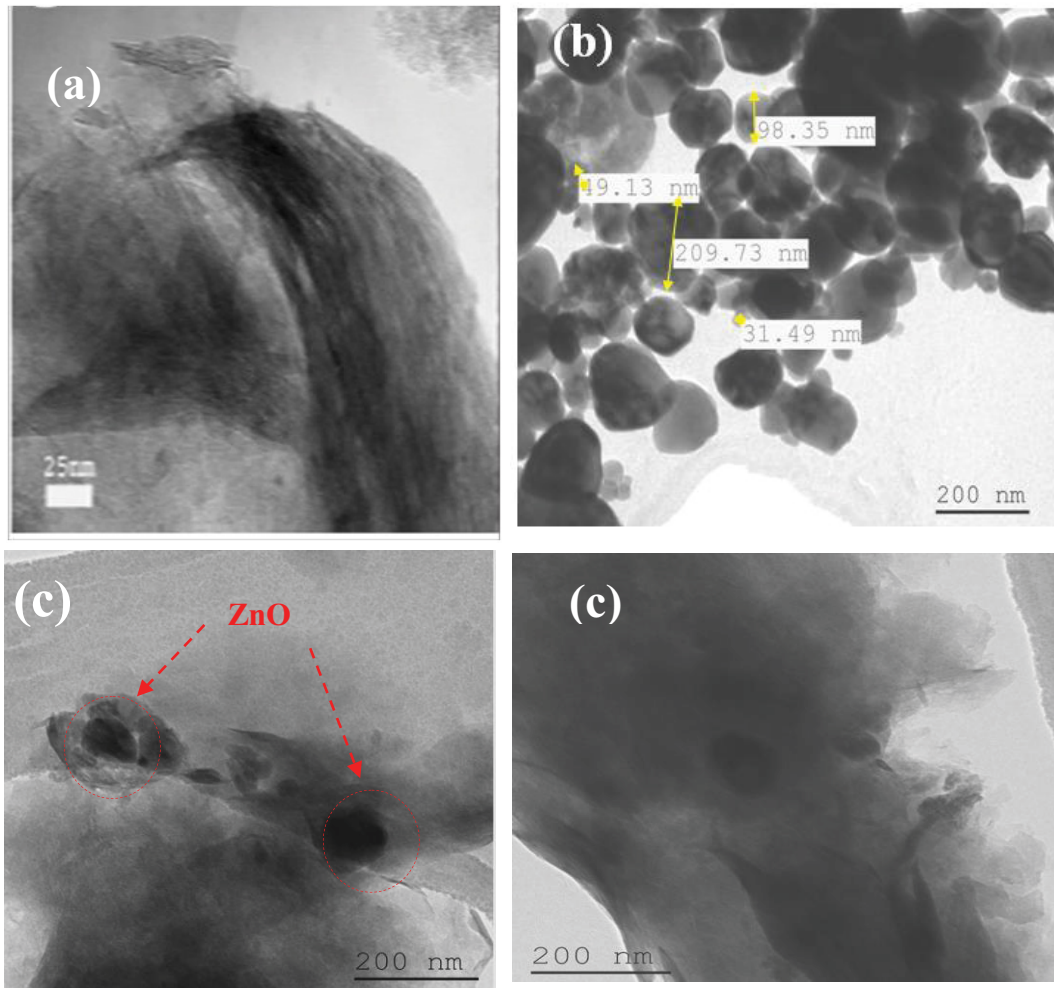


Fig. 2. TEM micrographs of pure clay (a), ZnO (b), and ZnO-clay (c).

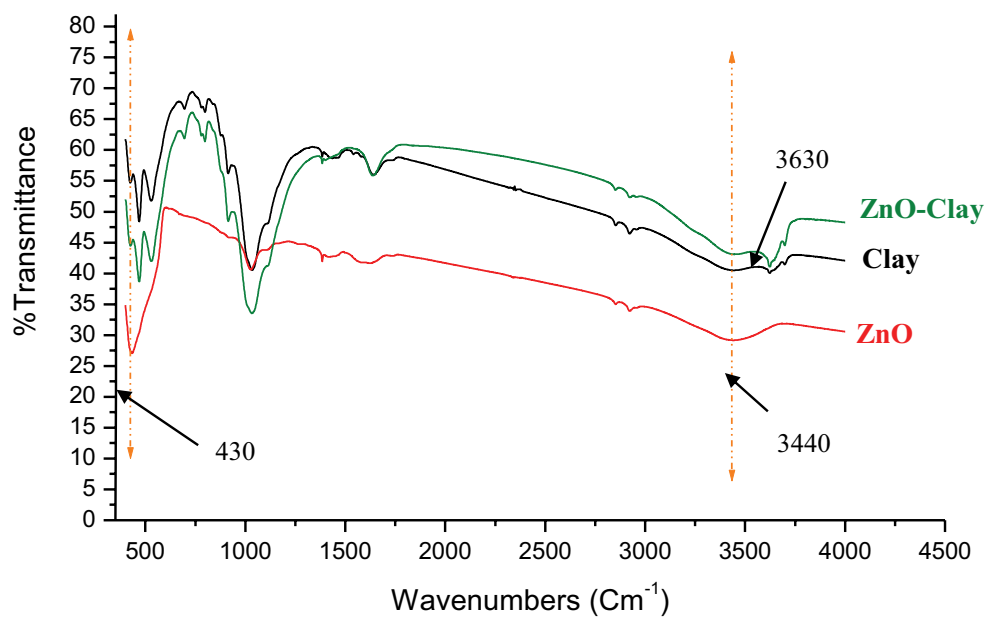


Fig. 3. Infrared spectra of pure clay, ZnO and ZnO-clay.

3.2.5. Adsorption kinetics

Since adsorption equilibrium time is a fundamental parameters in photocatalytic reaction, a kinetic study was carried out (Fig. 4) by varying contact time, adsorbent/adsorbate contact time, from 5 min to 120 min.

As results, percent of adsorption increases quickly in the first 30 min for all adsorbent then it remains constant after 60 min, indicating the state of equilibrium (Fig. 4). It should be noted from this kinetic study that 60 min is a sufficient period to establish the adsorption–desorption equilibrium by these adsorbents.

Adsorption percent of AO dye onto ZnO-clay is extremely higher than the others adsorbents. The maximum adsorption quantities of AO at equilibrium time are 16.6, 20.3 and 30 mg g⁻¹ for pure ZnO, clay and ZnO-clay, respectively. This is due to the high adsorptive capacity of clay and the large amount of sorption sites developed after ZnO modification. Similar results were obtained by Hadjltaiet et al. [35].

Pseudo-first-order [30] and pseudo-second-order [31] kinetic equations have been used in order to describe adsorption process. Results (Fig. 5, Table 3) show that these two kinetic models fit well with experimental data ($R^2 \approx 1$) suggested that adsorption process is based on physisorption and

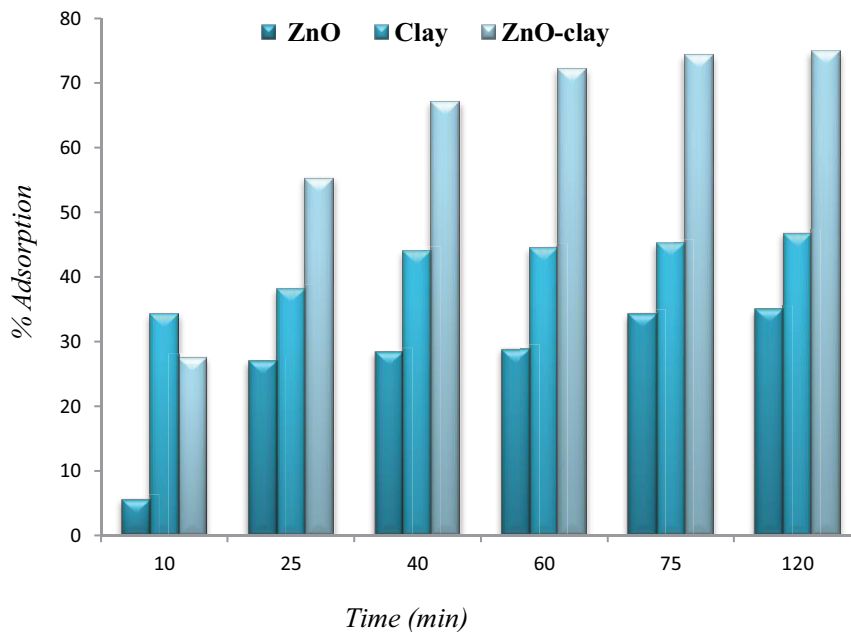


Fig. 4. Kinetics of AO dye adsorption onto pure clay, ZnO and ZnO-clay (pH = natural; $m = 0.1$ g; $V = 100$ mL; $[AO] = 10^{-4}$ M; $T = 25^\circ\text{C}$).

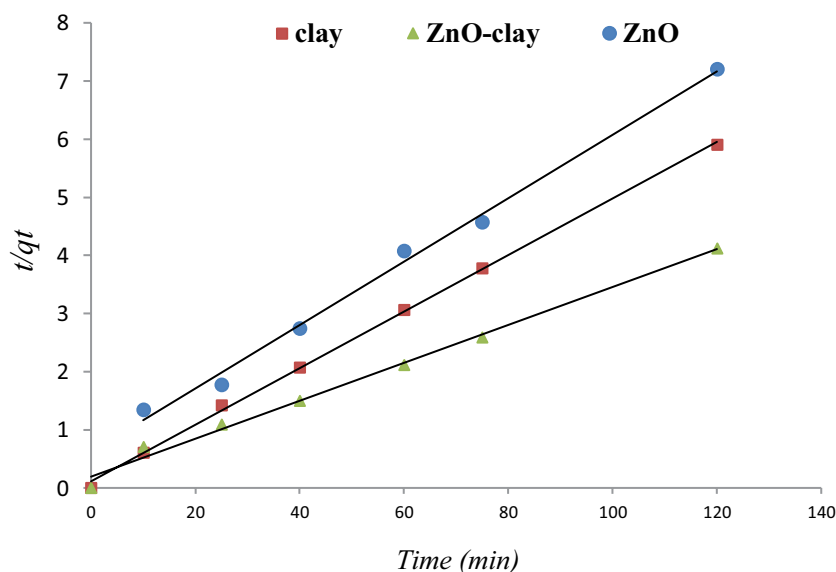


Fig. 5. Pseudo-second-order kinetic model of pure clay, ZnO and ZnO-clay (pH = natural; $m = 0.1$ g; $V = 100$ mL; $[AO] = 10^{-4}$ M; $T = 25^\circ\text{C}$).

chemisorptions mechanism [38], except with ZnO catalyst adsorption process is described only by pseudo-second-order model enhanced a physisorption process.

3.2.6. Photodegradation study of dye pollutant

Photocatalytic performance of ZnO nanoparticle, ZnO-clay nanocomposite and pure clay was evaluated by the photodegradation of Acridine orange dye under UV light irradiations (Fig. 6). As can be explained in section 3.2, the adsorption performance of the prepared catalysts was investigated by using the interaction of catalysts with AO dye and results confirm the good affinity between the pollutant and the photocatalyst which is considered a primordial key in photocatalytic reaction. For all the oxidation tests, an adsorption time of 1 h was established, guaranteeing conditions of adsorption–desorption equilibrium.

Table 3
Kinetics parameters of AO dye adsorption onto pure clay, ZnO and ZnO-clay

Pseudo-second-order			Pseudo-first-order	
K_2 (g g ⁻¹ min ⁻¹)	$q_{e,cal}$ (g g ⁻¹)	R^2	$q_{e,cal}$ (g g ⁻¹)	R^2
Pure clay				
0.02	20.83	0.999	9.49	0.942
ZnO				
0.0047	18.51	0.994	7.98	0.599
ZnO-clay				
31.25	0.0053	0.992	31.18	0.986

Results show that ZnO-clay photocatalyst was more sensitive to UV light for AO dye photodegradation (Fig. 6). As can be seen from Fig. 6 the photodegradation rate is 84.5% with ZnO-clay after 120 min irradiation, which is higher than that reached by ZnO nanoparticles (77.2%) and seven times more important than that achieved by pure clay (12.4%). This can be explained by the fact that pure clay having an important adsorption capacity for AO dye removal associated with the significant ZnO photocatalytic activities performance, gives together an hybrid catalyst with a highest photodegradation efficiency; ZnO-clay nanocomposite. Similar results were obtained by Hadjltaief et al. [35] confirming the enhancement of the photocatalytic activity using a bentonitic clay and a pure photocatalyst.

Photodegradation kinetic is analysed by the defined Langmuir–Hinshelwood (L-H) model [39]. As it was explained by Nguyen et al. [40], the L-H model states the proportionality between the degradation rate, v (mmol L⁻¹ min⁻¹) and the dye fraction coverage the photocatalyst surface, σ , and it was expressed as:

$$v = -\frac{dC_t}{dt} = K\sigma = \frac{KK_L C_t}{1 + K_L C_t} \quad (5)$$

where C_t : is the concentration of dye at time t ; K : is the rate constant; K_L : is the adsorption constant.

Considering the low concentration of dye pollutant or relatively weak adsorption ($K_L C_t \ll 1$), Eq. (6) can be simplified as follows:

$$\frac{dC_t}{dt} = -KK_L C_t = -K_{app} C_t \quad (6)$$

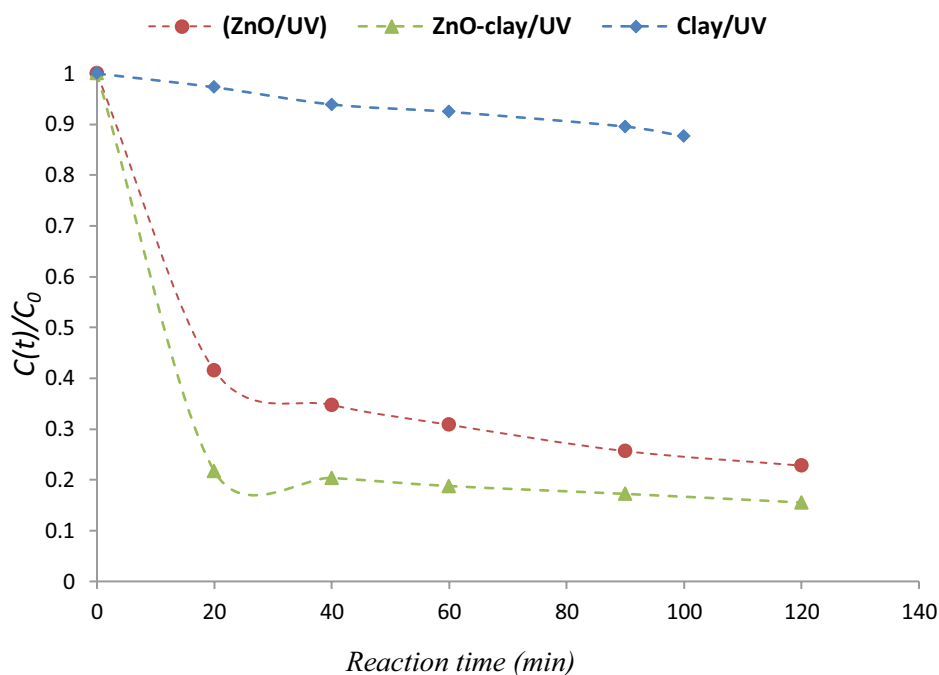


Fig. 6. Photodegradation of AO dye over ZnO, pure clay and ZnO-clay photocatalysts ($[AO]_0 = 10^{-4}$ mol L⁻¹; $pH_0 = 7$; $T = 25^\circ\text{C}$).

where K_{app} is the apparent first-order rate constant (min^{-1}). The integration of Eq. (6) gives the following equation:

$$\ln \frac{C_t}{C_0} = -K_{app}t \quad (7)$$

Modelisation of the experimental results of AO photodegradation by the investigated materials, using the L-H model shows that the first-order kinetics is suitable for this experience. Results (Table 4) show that ZnO-clay presents the highest constant rate ($K_{app} = 5 \times 10^{-3} \text{ min}^{-1}$), as well as pure ZnO ($K_{app} = 3 \times 10^{-3} \text{ min}^{-1}$) compared to pure clay ($1 \times 10^{-3} \text{ min}^{-1}$).

Therefore, under UV irradiations ZnO-clay photocatalyst showed both the highest photocatalytic activity and the maximum apparent kinetic constant.

For a better explanation of the photochemical removal of studied dye, photodegradation of AO was conducted under

different conditions in order to evaluate the contribution of each parameter. In Fig. 7 we show the different studied ways for AO degradation. Photolysis process illustrates 8% of dye degradation under UV light without the presence of any catalysts. In the case of UV light irradiation combined with H_2O_2 (UV/ H_2O_2), AO photodegradation efficiency increases to 92.5% because UV light catalysed H_2O_2 to generate HO. radicals according to Eq. (8).



A greater enhancement in photocatalytic degradation was achieved in the presence of H_2O_2 with (ZnO/UV) and (ZnO-clay/UV) systems, indicating 84.9% and 97.8% of photodegradation efficiency respectively. Indeed the major advantage of oxidant addition is that hydroxyl radicals are generated into the reaction system by photolysis of H_2O_2 under UV irradiations and the photocatalytic activity of the studied photocatalysts ZnO and ZnO-clay under UV irradiations.

To confirm the effectiveness of AO mineralisation via the investigated photocatalysts, a comparison study of photodegradation efficiency and COD analysis was determined at different reaction conditions (Fig. 7), irradiation time was fixed at 90 min. Results show that for both photocatalysts, under UV irradiations only, the AO dye mineralization degree attains 60% which is enhanced by the presence of H_2O_2 reaching 62.9% and 82.7% for ZnO and ZnO-clay respectively. We noted that with H_2O_2 /UV system the percent of COD removal reach 76.2%.

Table 4

Parameters of first-order kinetics of the AO dye photodegradation

Photocatalysts	Photodegradation (%)	$K_{app} \times 10^{-3} (\text{min}^{-1})$	R^2
Pure clay	12.4	1	0.97
ZnO	77.2	3	0.98
ZnO-clay	84.5	5	0.99

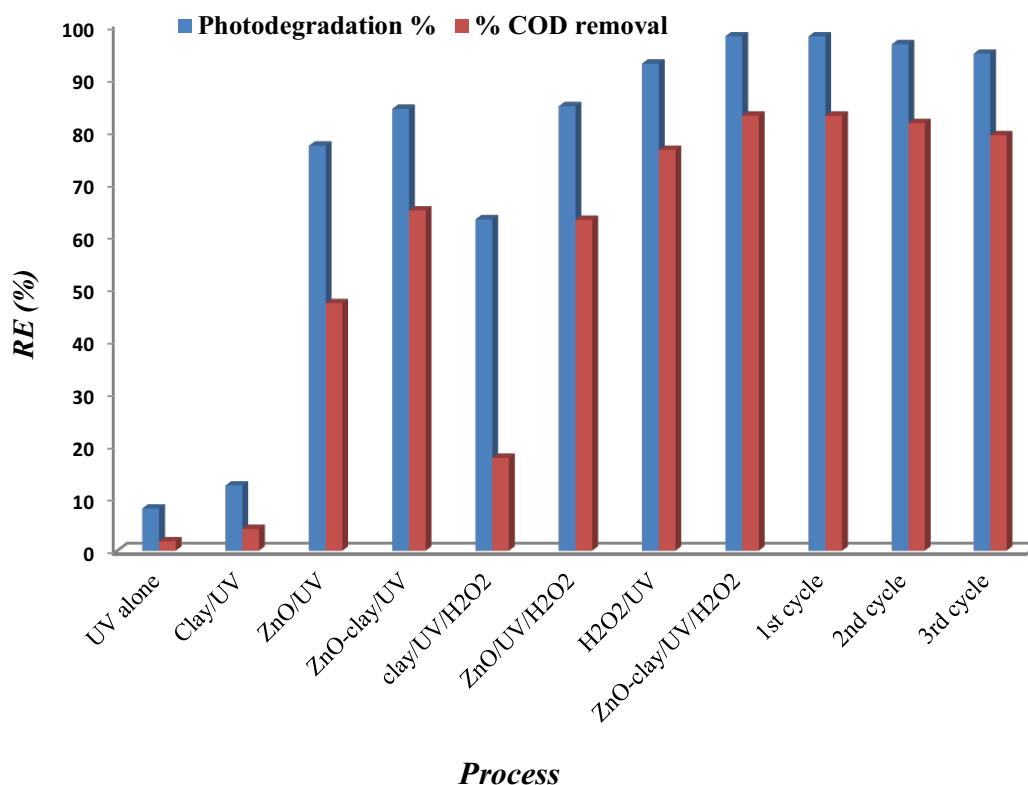


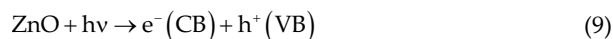
Fig. 7. Degree of AO dye degradation and mineralization by different ways ($[\text{AO}]_0 = 10^{-4} \text{ mol L}^{-1}$; $\text{pH}_0 = 7$; $T = 25^\circ\text{C}$).

Stability of ZnO-clay photocatalyst during successive photocatalytic reactions recycling tests was conducted. The photocatalyst used in the previous test was collected by centrifugation, washed several times with distilled water and then dried at 70°C for 24 h. 0.2 g mass of this material was taken into consideration for each test. The activity of this material is evaluated 3 times by addition of a fresh dye solution with the recovered photocatalyst of the preceding test under the following operating conditions: $[AO]_0 = 10^{-4} \text{ mol L}^{-1}$, $V_{H_2O_2} = 1 \text{ mL}$, $pH_0 = 7$ and $T = 25^\circ\text{C}$.

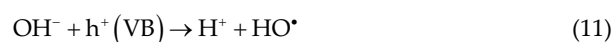
It can be clearly seen (Fig. 7) that there is no significant decrease in the photocatalytic activity of ZnO-clay after three successive cycles: the rate photodegradation of 94.5% against 97.8% at the time of the first use. These findings confirm the stability and the possibility of reusing ZnO-clay material for the removal of this textile dye.

It is known that in photocatalytic process using semiconductor as ZnO, hydroxyl radical can be generated by several ways. The most reported in literature are summarized as follows [35]:

- Photo-excitation of photocatalyst with light, enhancing the transfer of an electron e^- from the valence band (VB) to the conduction band (CB), which assure the leave of an electronic vacancy or hole h^+ in the valence band (VB) and thus the generation of an electron-hole pair:



- The oxidation of H_2O and OH^- by holes (h^+) formed in the valence band (VB):



- The reduction of O_2 by electrons photo-generated on semiconductor surface via the conduction band (CB) leading to the formation of $O_2^{\bullet-}$ radicals then HO^\bullet radicals, acting as it is reported in reactions sequences:



- Reactive oxygen species $O_2^{\bullet-}$ and HO^\bullet attack the adsorbed dye onto ZnO-clay surface conducting to their mineralization on CO_2 and H_2O (Fig. 8).

Degradation products formed at the end of irradiation process were analyzed by LC-MS technique. According to obtained results (Table 5, LC-MS spectrum were not presented) and from the data provided in the literature [7,41],

Table 5
N-de-methylated intermediates formed during the photodegradation of the AO dye after separation by LC-MS method

Product	N-de-methylation intermediates	LC-MS peaks (m/z)
1	Acridine orange (AO)	266.12
2	N-de-mono-methyl-AO	252.13
3	N,N'-de-dimethyl-AO	238.08
4	N,N'-de-dimethyl-AO	238.14
5	N,N,N'-de-trimethyl-AO	224.09
6	N,N,N',N'-de-tetramethyl-AO	210.04

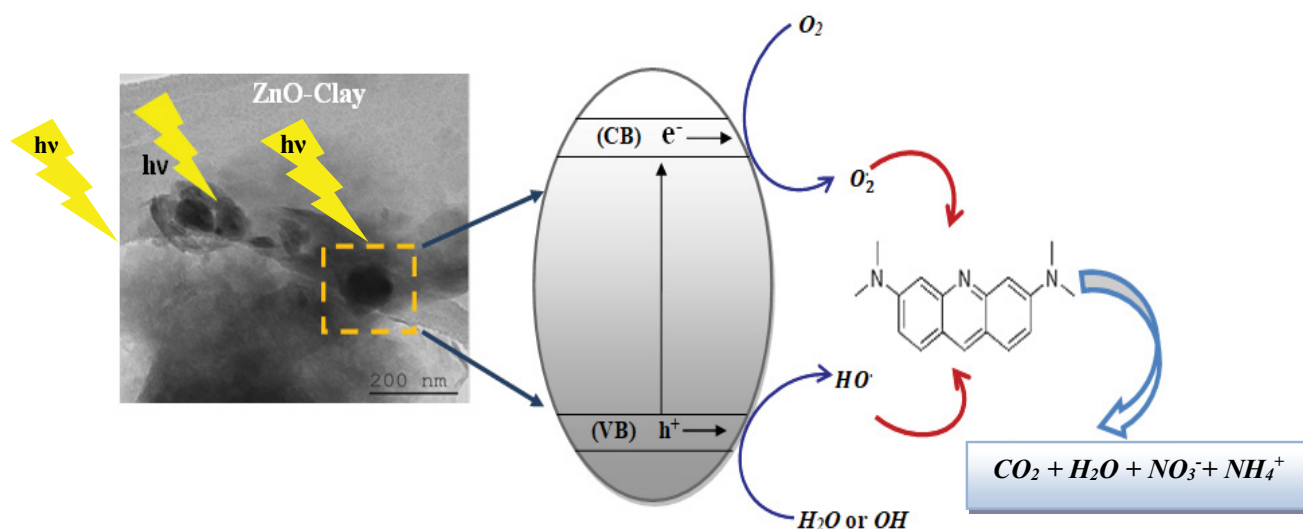


Fig. 8. Mechanism of photocatalytic degradation of Acridine orange dye by ZnO-clay as photocatalyst.

a pathway can be proposed for the Acridine orange degradation (Fig. 9).

Acridine orange dye degradation can occur via the following mechanism: beginning by the remove of methyl groups one by one until formation of the completely N-de-methylated dye and finally, this organic compound was mineralized to inorganic ions, CO_2 and H_2O . Similar

results were obtained by Lu et al. [41] which described the mechanism of AO degradation by Fenton process in aqueous medium by the N-de-methylation reaction. Also, Chen et al. [7] in their work were studied the degradation of AO dye by TiO_2 under UV light irradiation and defined the N-de-methylation reaction pathway for dye degradation.

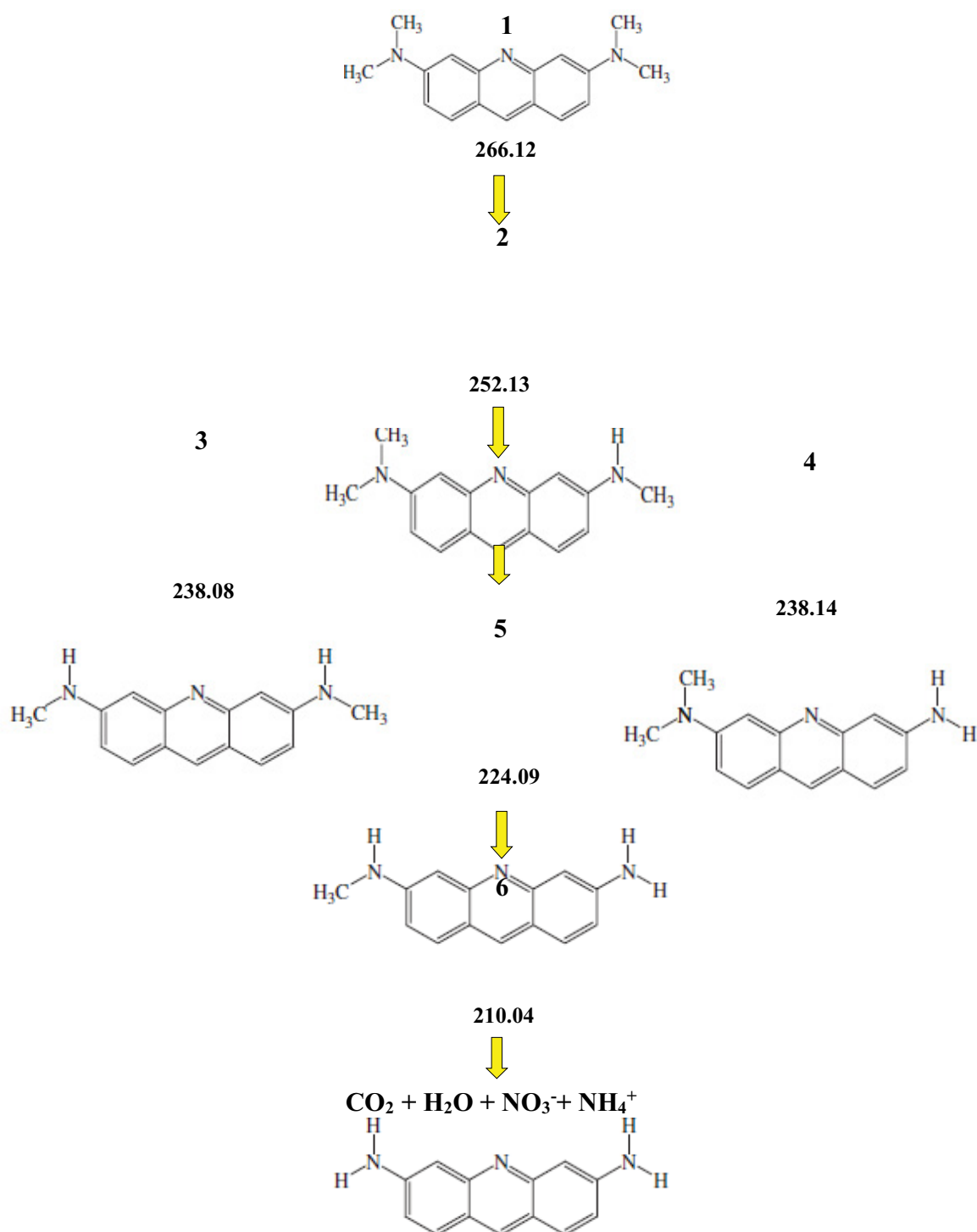


Fig. 9. Proposed degradation pathway of Acridine orange dye under UV light irradiation.

3.3. Comparison of degradation efficiency of Acridine orange dye with literature

In this section, a comparative study between this work and literature was established regarding the application of different photocatalysts for organic pollutants degradation. For this purpose, Table 6 illustrates the results obtained in term of degradation efficiency in the presence of synthesized material ZnO-clay used in this work and other catalysts mentioned in published works. According to these results, we can conclude the efficiency and the good activity of the investigated material which specify the importance of this work in the research.

3.4. Real wastewater treatment

According to above-mentioned results, in this section we are interested to the photodegradation of a real textile effluent under the optimal conditions and we presented the most physicochemical characteristics before and after treatment. The sample was collected from the effluent of local textile industry (SITEX company; east of Tunisia) specialized in yarn manufacturing, indigo dyeing process and textile finishing, before being subjected to any form of treatment. Water sample was filtered before use. An amount of 0.2 g of ZnO-clay photocatalyst was added to 150 mL of effluent sample. This mixture was shaken for 1 h in the dark at room temperature (25°C) to ensure the adsorption-desorption equilibrium, then 1 mL of H₂O₂ oxidant was added and the lamp UV was turn ON. Table 7 shows the most characteristic of the effluent before and after 3 h

of treatment with photocatalyse reaction under ultraviolet irradiations.

The photocatalytic activity of the prepared photocatalyst ZnO-clay under UV irradiation clearly indicates a good performance of this material for real wastewater treatment. As can be seen from table, physicochemical quality indicators of effluents decrease considerably compared to them before treatment. The pH reaches a neutral value; therefore, it can be released in aquatic medium (6 < pH < 8.5) [42]). Also, it is the case for COD value (65.53% of COD removal) respects the condition for releasing in public sewage systems, yet in aquatic environment. Also, the color removal was achieved 80.2% which is considered an efficient result.

4. Conclusion

Photocatalyst based on ZnO modified clay nanocomposite was synthesised and investigated in this study for Acridine orange dye photodegradation. Pure clay, ZnO and ZnO-clay were characterized by different techniques like XRD, TEM analysis, textural analysis. Adsorption experiments were conducted to study the affinity between investigated material and AO dye. Adsorption experiments were studied and both pseudo-second-order and pseudo-first-order for kinetics models fitted the Acridine orange adsorption data except with pure ZnO catalyst adsorption process is described only by pseudo-second-order model. The influence of different conditions of the photocatalytic process (under UV irradiation and presence of H₂O₂ oxidant) on the efficiency of AO dye degradation was established. Experimental data indicated that

Table 6
Comparison of catalytic activity for different catalysts

Catalyst	Pollutant	% degradation	Reference
ZnO-TiO ₂ /clay	Methyl green	89.3	[29]
ZnO-clay	Acridine orange	97.82	This work
ZnO	Acridine orange	85	This work
ZnO-clay	Malachite green	97.18	[35]
	Congo red	97.6	
Activated carbon supported titania	Phenol	77	[7]
ZnO	Acridine orange	90	[6]

Table 7
Most characteristics of real wastewater before and after photo-treatment with ZnO-clay/UV/H₂O₂ system

Parameters	Before treatment	After treatment	Tunisian Standard (for river discharge) [42]
pH	12.4	8.5	6.5–8.5
BOD ₅	600	90	30
COD	1,300	448.1	90
Color	3,500	190	70
Suspended solids	200	traces	30
Total hardness	100	traces	5
Oil and grease	10	traces	20
Chloride	1,700	600	600

Except pH, the units of all other parameters are mg L⁻¹.

ZnO-clay was an efficient photocatalyst under UV irradiation and in the presence of H₂O₂ oxidant (around 97.8% of Acridine orange removal and 82.7% mineralization were achieved after 90 min). The photocatalytic reaction followed pseudo-first-order kinetics and the apparent rate constant increased with photocatalyst performance. The N-de-methylation degradation was defined as reaction mechanism of AO dye degradation. Above-mentioned discussions indicate that the prepared catalyst exhibits good photocatalytic activities on degradation and mineralization of AO dye in aqueous solution. Furthermore, the conducted research has shown the practical application of the developed material for real textile wastewater treatment.

Acknowledgment

This work was supported by the Research Supporting Project (RSP- 2021/75), King Saud University (Riyadh, Saudi Arabia).

References

- [1] T. Ochiai, A. Fujishima, Photoelectrochemical properties of TiO₂ photocatalyst and its applications for environmental purification, *J. Photochem. Photobiol., C*, 13 (2012) 247–262.
- [2] M.N. Chong, B. Jin, C.W.K. Chow, C. Saint, Recent developments in photocatalytic water treatment technology: a review, *Water Res.*, 44 (2010) 2997–3027.
- [3] F. Mijangos, F. Varona, N. Villota, Changes in solution color during phenol oxidation by Fenton reagent, *Environ. Sci. Technol.*, 40 (2006) 5538–5543.
- [4] S. Esplugas, J. Giménez, S. Contreras, E. Pascual, M. Rodríguez, Comparison of different advanced oxidation processes for phenol degradation, *Water Res.*, 36 (2002) 1034–1042.
- [5] E. Neyens, J. Baeyens, A review of classic Fenton's peroxidation as an advanced oxidation technique, *J. Hazard. Mater.*, 98 (2003) 33–50.
- [6] B. Pare, S.B. Jonnalagadda, H. Tomar, P. Singh, V.W. Bhagwat, ZnO assisted photocatalytic degradation of Acridine orange in aqueous solution using visible irradiation, *Desalination*, 232 (2008) 80–90.
- [7] C.-C. Chen, R.-J. Wu, Y.-Y. Tzeng, C.-S. Lu, Chemical oxidative degradation of Acridine orange dye in aqueous solution by Fenton's reagent, *J. Chin. Chem. Soc. Taipei*, 56 (2009) 1147–1155.
- [8] A. Maleki, M. Safari, B. Shahmoradi, Y. Zandsalimi, H. Daraei, F. Gharibi, Photocatalytic degradation of humic substances in aqueous solution using Cu-doped ZnO nanoparticles under natural sunlight irradiation, *Environ. Sci. Pollut. Res.*, 22 (2015) 16875–16880.
- [9] H.K. Farag, R.M.M. Aboelenin, N.A. Fathy, Photodegradation of methyl orange dye by ZnO loaded onto carbon xerogels composites, *Asia-Pacific J. Chem. Eng.*, 12 (2017) 4–12.
- [10] I.M. Jauris, S.B. Fagan, M.A. Adebayo, F.M. Machado, Adsorption of Acridine orange and Methylene blue synthetic dyes and anthracene on single wall carbon nanotubes: a first principle approach, *Comput. Theor. Chem.*, 1076 (2016) 42–50.
- [11] S.K.H. Nejad-Darzi, A. Samadi-Maybodi, M. Ghobakhluo, Synthesis and characterization of modified ZSM-5 nanozeolite and their applications in adsorption of Acridine orange dye from aqueous solution, *J. Porous Mater.*, 20 (2013) 909–916.
- [12] E. Chamarro, A. Marco, S. Esplugas, Use of Fenton reagent to improve organic chemical biodegradability, *Water Res.*, 35 (2001) 1047–1051.
- [13] S. Chiron, A. Fernandez-Alba, A. Rodriguez, E. Garcia-Calvo, Pesticide chemical oxidation: state-of-the-art, *Water Res.*, 34 (2000) 366–377.
- [14] R.C.C. Costa, M.F.F. Lelis, L.C.A. Oliveira, J.D. Fabris, J.D. Ardisson, R.R.V.A. Rios, C.N. Silva, R.M. Lago, Novel active heterogeneous Fenton system based on Fe_{3-x}M_xO₄ (Fe, Co, Mn, Ni): the role of M²⁺ species on the reactivity towards H₂O₂ reactions, *J. Hazard. Mater.*, 129 (2006) 171–178.
- [15] S. Sabhi, J. Kiwi, Degradation of 2,4-dichlorophenol by immobilized iron catalysts, *Water Res.*, 35 (2001) 1994–2002.
- [16] H. Shemer, Y.K. Kunukcu, K.G. Linden, Degradation of the pharmaceutical metronidazole via UV, Fenton and photo-Fenton processes, *Chemosphere*, 63 (2006) 269–276.
- [17] I. Oller, S. Malato, J. Sánchez-Pérez, Combination of advanced oxidation processes and biological treatments for wastewater decontamination—a review, *Sci. Total Environ.*, 409 (2011) 4141–4166.
- [18] S.G. Schrank, J.N.R. dos Santos, D.S. Souza, E.E.S. Souza, Decolourisation effects of Vat Green 01 textile dye and textile wastewater using H₂O₂/UV process, *J. Photochem. Photobiol., A*, 186 (2007) 125–129.
- [19] R. Byberg, J. Cobb, L. Diez Martin, R.W. Thompson, T.A. Camesano, O. Zahraa, M.N. Pons, Comparison of photocatalytic degradation of dyes in relation to their structure, *Environ. Sci. Pollut. Res.*, 20 (2013) 3570–3581.
- [20] P.A. Pekakis, N.P. Xekoukoulotakis, D. Mantzavinos, Treatment of textile dyehouse wastewater by TiO₂ photocatalysis, *Water Res.*, 40 (2006) 1276–1286.
- [21] S. In, A. Orlov, R. Berg, F. Garcia, S. Pedrosa-Jimenez, M.S. Tikhov, D.S. Wright, R.M. Lambert, Effective visible light-activated B-doped and B, N-co-doped TiO₂ photocatalysts, *J. Am. Chem. Soc.*, 129 (2007) 13790–13791.
- [22] S. Karthikeyan, A. Titus, A. Gnanamani, A.B. Mandal, G. Sekaran, Treatment of textile wastewater by homogeneous and heterogeneous Fenton oxidation processes, *Desalination*, 281 (2011) 438–445.
- [23] P.V. Nidheesh, R. Gandhimathi, S.T. Ramesh, Degradation of dyes from aqueous solution by Fenton processes: a review, *Environ. Sci. Pollut. Res.*, 20 (2013) 2099–2132.
- [24] A.N. Módenes, F.R. Espinoza-Quiñones, F.H. Borba, D.R. Manenti, Performance evaluation of an integrated photo-Fenton – electrocoagulation process applied to pollutant removal from tannery effluent in batch system, *Chem. Eng. J.*, 197 (2012) 1–9.
- [25] H. Lin, H. Zhang, X. Wang, L. Wang, J. Wu, Electro-Fenton removal of Orange II in a divided cell: reaction mechanism, degradation pathway and toxicity evolution, *Sep. Purif. Technol.*, 122 (2014) 533–540.
- [26] H. Chaker, L. Chérif-Aouali, S. Khaoulani, A. Bengueddach, S. Fourmentin, Photocatalytic degradation of methyl orange and real wastewater by silver doped mesoporous TiO₂ catalysts, *J. Photochem. Photobiol., A*, 318 (2016) 142–149.
- [27] S. Khelifi, F. Ayari, Modified bentonite for anionic dye removal from aqueous solutions. Adsorbent regeneration by the photo-Fenton process, *C.R. Chim.*, 22 (2019) 154–160.
- [28] F. Ayari, A.B. Othmen, S. Khelifi, M. Trabelsi-Ayadi, Photodegradation of Congo red and real textile industries effluent using natural Tunisian iron oxide, *Desal. Water Treat.*, 107 (2018) 316–323.
- [29] H.B. Hadjiltaief, M.B. Zina, M.E. Galvez, P. Da Costa, Photocatalytic degradation of Methyl green dye in aqueous solution over natural clay-supported ZnO–TiO₂ catalysts, *J. Photochem. Photobiol., A*, 315 (2016) 25–33.
- [30] R. Tanwar, S. Kumar, U.K. Mandal, Photocatalytic activity of PANI/Fe⁰ doped BiOCl under visible light-degradation of Congo red dye, *J. Photochem. Photobiol., A*, 333 (2017) 105–116.
- [31] V. Ponnusami, V. Gunasekar, S.N. Srivastava, Kinetics of methylene blue removal from aqueous solution using gulmohar (*Delonix regia*) plant leaf powder: multivariate regression analysis, *J. Hazard. Mater.*, 169 (2009) 119–127.
- [32] G. Brown, Crystal Structures of Clay Minerals and Their X-ray Identification, The Mineralogical Society of Great Britain and Ireland, Vol. 5, 1982.
- [33] S.-Q. Li, P.-J. Zhou, W.-S. Zhang, S. Chen, H. Peng, Effective photocatalytic decolorization of methylene blue utilizing ZnO/

- rectorite nanocomposite under simulated solar irradiation, *J. Alloys Compd.*, 616 (2014) 227–234.
- [34] H. Xu, D. Zhang, A. Xu, F. Wu, R. Cao, Quantum sized zinc oxide immobilized on bentonite clay and degradation of C.I. acid red 35 in aqueous under ultraviolet light, *Int. J. Photoenergy*, 2015 (2015) 750869, doi: 10.1155/2015/750869.
- [35] H.B. Hadjltaief, S.B. Ameer, P. Da Costa, M.B. Zina, M.E. Galvez, Photocatalytic decolorization of cationic and anionic dyes over ZnO nanoparticle immobilized on natural Tunisian clay, *Appl. Clay Sci.*, 152 (2018) 148–157.
- [36] F. Ayari, E. Srasra, M. Trabelsi-Ayadi, Retention of lead from an aqueous solution by use of bentonite as adsorbent for reducing leaching from industrial effluents, *Desalination*, 206 (2007) 270–278.
- [37] S.C. Motshekga, S.S. Ray, M.S. Onyango, M.N.B. Momba, Microwave-assisted synthesis, characterization and anti-bacterial activity of Ag/ZnO nanoparticles supported bentonite clay, *J. Hazard. Mater.*, 262 (2013) 439–446.
- [38] F. Ayari, G. Manai, S. Khelifi, M. Trabelsi-Ayadi, Treatment of anionic dye aqueous solution using Ti, HDTMA and Al/Fe pillared bentonite. Essay to regenerate the adsorbent, *J. Saudi Chem. Soc.*, 23 (2019) 294–306.
- [39] Y.F. Wang, J.H. Zhang, X.L. Chen, X. Li, Z.Q. Sun, K. Zhang, Morphology-controlled fabrication of polygonal ZnO nanobowls templated from spherical polymeric nanowell arrays, *J. Colloid Interface Sci.*, 322 (2008) 327–332.
- [40] C.H. Nguyen, H.N. Tran, C.-C. Fu, Y.-T. Lu, R.-S. Juang, Roles of adsorption and photocatalysis in removing organic pollutants from water by activated carbon-supported titania composites: kinetic aspects, *J. Taiwan Inst. Chem. Eng.*, 109 (2020) 51–61.
- [41] C.-S. Lu, F.-D. Mai, C.-W. Wu, R.-J. Wu, C.-C. Chen, Titanium dioxide-mediated photocatalytic degradation of Acridine orange in aqueous suspensions under UV irradiation, *Dyes Pigm.*, 76 (2008) 706–713.
- [42] NT 106.02 TS-BojbtMotNE, Implementing the TUNISIAN Standard Concerning Wastewater Effluent Discharges in the Hydrous Medium, 1989, p. 1332.